


Comparative analysis and improved design of LLC inverters for induction heating

Vicente Esteve¹  | José Jordán¹ | Enrique J. Dede¹ | Pedro J. Martínez² |
Kevil J. Ferrara² | Juan L. Bellido²

¹Department of Electronic Engineering, University of Valencia, Valencia, Spain

²R&D Department, SiCtech Induction, Paterna, Spain

Correspondence

Vicente Esteve, Department of Electronic Engineering, University of Valencia, Av. University s/n, Valencia 46100, Spain.
Email: vesteveg@uv.es

Abstract

This work presents a comparative analysis and design procedure of a converter based on an LLC resonant inverter used for induction heating applications depending on the transistor technology used and the selected operating frequency. A major objective of the work is to determinate the inverter design requirements leading to the optimal sizing of the components, improving its operation and minimizing power losses. Additionally, it proposes a design to obtain a great insensitivity of the inverter operation against large variations of load impedance. This article analyzes the operation of the inverter where the power regulation is carried out by phase-shift (PS) modulation. Simple rules are formulated for the design of the resonant circuit components. The design has been verified testing a 25-kW inverter in an industrial application of induction hardening operating at 500 kHz. Inverter efficiency is around 98.5% when using Silicon Carbide (SiC) MOSFETs.

1 | INTRODUCTION

Induction heating is a heat treatment used in several industrial applications [1]. The part to be heated, called work-piece, is placed in a magnetic field generated by a coil, called heating inductor, that is fed by using a high current and high frequency power supply [2]. The Foucault or eddy currents induced in the surface of the work-piece originate the heat due to Joule and hysteresis losses. The depth of the heated zone, called penetration depth δ , depends on the current frequency due to the skin effect as well as the heat conduction property. Higher operating frequencies have a shallow skin depth, while lower operating frequencies have a thicker skin depth and greater depth of penetration [3].

The load of induction heating converters is formed by the heating inductor and its equivalent loss resistance which may be connected in series or parallel depending on the model. In order to compensate the reactive energy of the load, a capacitor is added resulting in this way a resonant load. The capacitor may be connected in series, in series resonant inverters (SRI) [4–6] or in parallel, in parallel resonant inverters (PRI) [7–9]. Both are used for forging, welding, melting, hardening and more metal heat treatment applications.

SRI power regulation can be made through phase shift (PS) [12, 13], pulse frequency modulation (PFM) [10, 11], or pulse density modulation (PDM) [14, 15]. SRI output current should be boosted by using transformers. PRI can achieve high inductor currents without a matching transformer, but they normally need a regulated current input source to control the output power. PRI inverters are complex and expensive circuits with a large input inductance that acts as a current source. The topological position of this inductance can be changed at the output of the inverter, in series with the parallel resonant circuit, resulting in an LLC resonant inverter that maintains PRI properties using a simple DC input voltage source, easily achievable power control strategies and with a good behaviour in front of short circuit [16–18]. Note that the output power factor of the circuit is determined by the inductance L_s , even in parallel resonance, increasing the stress of the components.

The previously published studies determined that the operation of the LLC inverter is based on switching near the input resonant frequency of the LLC circuit [17, 18]; however, in these conditions the output current values and the stress of the power components are high compared to the SRI inverter. The main objective of this work is to find the optimal design LLC inverter. This optimization consists of obtaining a reduction of

This is an open access article under the terms of the [Creative Commons Attribution](https://creativecommons.org/licenses/by/4.0/) License, which permits use, distribution and reproduction in any medium, provided the original work is properly cited.

© 2023 The Authors. *IET Power Electronics* published by John Wiley & Sons Ltd on behalf of The Institution of Engineering and Technology.

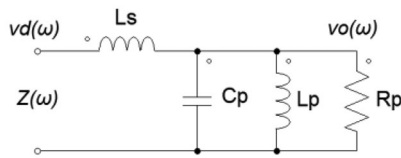


FIGURE 1 LLC resonant circuit.

the square root of the mean square (RMS) inverter output current to minimize conduction losses in the entire power circuit: transistors, conductors, capacitor and inductors. Also, it reduces the switching current to decrease losses in the transistors.

After making an inverter comparative study according to the transistor technology and the switching frequency selected, this paper will present an LLC inverter design procedure where the operating frequency is chosen in order to get optimal inverter operation. In addition, it will be verified that the operation of the LLC inverter at this working frequency is very insensitive to large changes in the load impedance compared to the operation of the classic inverter.

The article is divided into the following sections: Section 2 provides the LLC resonant circuit state of art applied to an induction heating application. Section 3 shows a design method to work at different frequencies based on the configuration and operation of the LLC inverter. Section 4 presents the comparative analysis results with different transistor technologies and working frequencies. Section 5 introduces the phase-shift (PS)-based power control system, analyzing its operation and making a comparative power loss study, and Section 6 demonstrates the viability of the PS control system with experimental results.

2 | THE LLC RESONANT CIRCUIT

Three reactive components make possible the LLC resonant circuit configuration, two inductors and a capacitor (LLC), connected with the equivalent load resistance as shown in Figure 1.

The LLC circuit can be considered a series-parallel hybrid. The input inductance acts like a current source connected to a voltage-fed inverter which simplifies the input section of the converter similar to SRI. The output has a capacitor in parallel as in parallel resonant circuits. All this will help to maintain some of the most advantageous of both circuits.

The specifications for the design of the inverter will be obtained by solving a specific application. In this case it is a surface hardening application. Single-shot hardening systems employ the use of rotated components in the inductor, and the entire area is heated at the same time for a pre-determined amount of time. The induction heating system must be designed taking into account the particular specifications of the application, that is, the characteristics of the part to be heated, the depth of penetration and the geometry of the inductor. The working frequency, which must be close to resonance, and the inverter power is determined using design procedures based

TABLE 1 Hardening application specifications

Magnitude	Symbol	Value	Unit
Material		1040 carbon steel	
Penetration depth	δ	2	mm
Heating time	T	3	s
Work-piece diameter	WD	100	mm
Heating length	HL	5	mm
Inductor turns	N	1	
Inductor diameter	ID	120	mm

TABLE 2 Results obtained for the application

Magnitude	Symbol	Value	Unit
Operation frequency	f	450	kHz
Heated area	HS	1571	mm ²
Surface power density	σP	15.5	W/mm ²
Inverter output power	P_o	25	kW

TABLE 3 Parallel resonant components

Magnitude	Symbol	Value	Unit
Inductor inductance	L_p	0.5	μH
Quality factor	Q_p	6	
Equivalent parallel resistor	R_p	8.45	Ω
Inductor and capacitor voltage	v_o	460	V_{RMS}
Resonant capacitor	C	0.25	μF

on data obtained in previous studies [2, 19]. Table 1 shows the starting data and the results obtained, for example, of a single-shot hardening application over a cylindrical piece of steel. The parameters of the hardening, the heating time and dimensions of the part and the inductor have been chosen freely.

Based on the works of Lozinskii [19], from the penetration depth and the heating time we can obtain the working frequency f and the surface density of power σP necessary to cover the application. Once the heating surface, calculated as $HS = \pi \cdot WD \cdot HL$, has been determined, the total inverter output power required can be obtained whose value $P_o = \sigma P \cdot HS$. Table 2 shows the results obtained.

These results allow the calculation of the parallel resonant circuit components considered as the LLC output stage, which are shown in Table 3. The value of the heating inductor inductance L_p is obtained from its geometric parameters [20, 21]. The value of the parallel resonant circuit quality factor Q_p depends on many other factors such as the gap distance between the inductor and the surface of the work-piece, the working frequency and the electrical and magnetic characteristics of the material to be heated, which are a function of its temperature. From previous experiences in the application, we can determine

a value of $Q_p = 6$, constant in practice before exceeding the Curie temperature of the material [22]. Operating close to the parallel resonant frequency ($f \approx f_{op}$), Q_p is determined by

$$Q_p = \frac{R_p}{L_p \omega_{op}} \quad (1)$$

where $\omega_{op} = 2\pi f_{op}$. If we neglect the losses in the parasitic components of the circuit, the inverter power is dissipated in the equivalent resistance of the resonant circuit and therefore the voltage v_o across the resonant capacitor can be obtained as

$$v_o = \sqrt{P_o R_p} \quad (2)$$

The value of the resonant capacitor can be calculated with

$$C = \frac{1}{\omega_{op}^2 L_p} \quad (3)$$

Table 3 shows the summary of the results obtained.

Based on these starting data, the input impedance $Z(\omega)$ of the LLC resonant circuit can be written as [23]

$$Z(\omega) = L_p \beta \omega_{op} \frac{\frac{1}{\beta} - \left(\frac{\omega}{\omega_{op}}\right)^2 + j Q_p \frac{\omega}{\omega_{op}} \left[\frac{\beta+1}{\beta} - \left(\frac{\omega}{\omega_{op}}\right)^2\right]}{Q_p \left[1 - \left(\frac{\omega}{\omega_{op}}\right)^2\right] + j \frac{\omega}{\omega_{op}}} \quad (4)$$

where ω is the operating angular frequency and β is the ratio between the inductances

$$\beta = \frac{L_s}{L_p} \quad (5)$$

The voltage gain $H_v(\omega)$ is the relationship between the heating inductor voltage $v_o(\omega)$ and the inverter output voltage $v_d(\omega)$ (see Figure 1) which can be expressed as

$$H_v(\omega) = \frac{v_o(\omega)}{v_d(\omega)} = \frac{Z(\omega) - j L_s \omega}{Z(\omega)} \quad (6)$$

which means that the heating inductor voltage can be designed as a function of the factor β .

Figure 2 shows the frequency response of the main quantities that describe the LLC circuit.

With the impedance plots shown in Figure 2 the following can be concluded

- The real part of the impedance has its maximum at the parallel resonant frequency ω_{op} .
- The real part of the admittance has its maximum at the equivalent resonant frequency ω_o .
- There is a minimum in the impedance argument at a frequency ω_m between the two frequencies above.

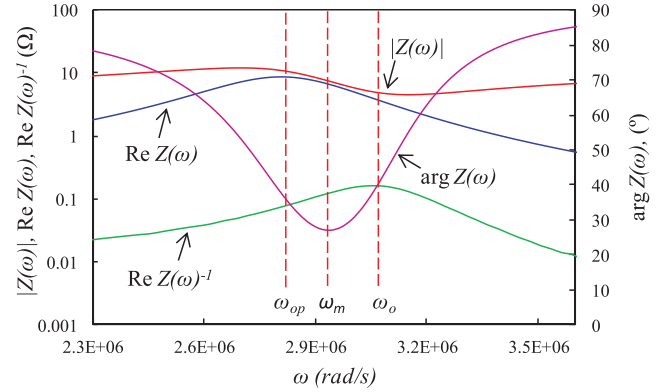


FIGURE 2 Impedance module (red), impedance argument (magenta), real part of impedance (blue) and real part of admittance (green) of the circuit resonant LLC.

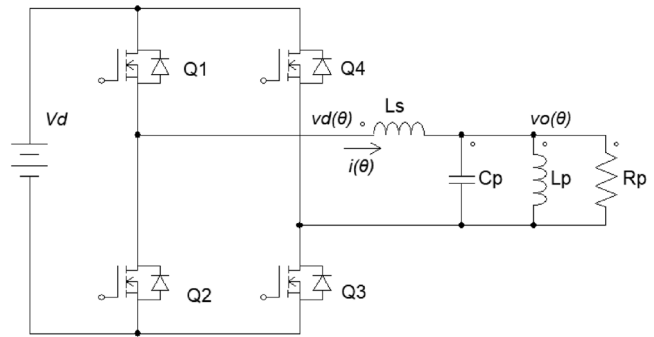


FIGURE 3 LLC resonant inverter.

With these assumptions the optimal operating point can be deduced. Working near ω_{op} the inverter output current will be reduced and near ω_o the maximum possible power will be obtained. In both cases the phase is relatively large and this makes the inverter current values (RMS and switching) high; however, operating near the minimum of the impedance argument, an optimal output power factor could be achieved.

It is also necessary to analyze the behaviour of the circuit against change in its equivalent resistance R_p (change of Q_p), as occurs when the part inside the heating inductor moves quickly or when the Curie temperature of the material is exceeded in heat treatment processes. In the following sections, we proceed to carry out a complete comparative study of the working conditions in each case to choose the optimal working condition of the LLC inverter.

3 | RESONANT LLC INVERTER DESIGN

The LLC inverter is composed of an H-bridge circuit fed by DC voltage and an LLC resonant circuit connected to its output as shown in Figure 3.

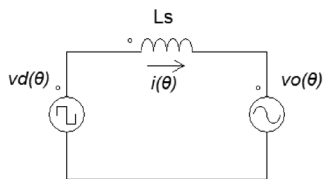


FIGURE 4 Equivalent circuit of resonant inverter LLC.

For high enough values of Q_p the output voltage $v_o(\theta)$ has an approximated sinusoidal value

$$v_o(\theta) = V_p \sin(\theta) \quad (7)$$

where V_p is the peak value of $v_o(\theta)$. Thus, the resulting simplified circuit is shown in Figure 4.

From the analysis of the circuit shown in Figure 4 the following equation can be written:

$$v_d(\theta) - v_o(\theta) = L_s \frac{d}{dt} i(\theta) \quad (8)$$

where $v_d(\theta)$ is

$$v_d(\theta) = \begin{cases} V_d & \text{if } 0 \leq \theta < \pi \\ -V_d & \text{if } \pi \leq \theta < 2\pi \end{cases} \quad (9)$$

Integrating (8) and solving the integration constants in order to have a continuous function, it can be obtained

$$i(\theta) = \begin{cases} \frac{V_d}{L_s \omega} \left(\theta + n \cos(\theta + \phi) - \frac{\pi}{2} \right) & \text{if } 0 \leq \theta < \pi \\ \frac{-V_d}{L_s \omega} \left(\theta - n \cos(\theta + \phi) - \frac{3\pi}{2} \right) & \text{if } \pi \leq \theta < 2\pi \end{cases} \quad (10)$$

where $n = V_p/V_d = 1.2$ with $V_d = 540$ V and ϕ is the phase between the resonant output voltage v_o and the inverter output voltage v_d that can be calculated with

$$\phi = \arg(H_v(\omega)) \quad (11)$$

When the operating frequency is close to the resonant frequency, only the RMS values of the first harmonics of the voltage involved in the circuit can be considered for the calculation of the voltage gain and, therefore, the following equality is fulfilled.

$$|H_v| = \frac{V_p/\sqrt{2}}{4V_d/\pi\sqrt{2}} = n \frac{\pi}{4} \quad (12)$$

To analyze the operation of the LLC inverter in each of the three frequencies mentioned in the previous section, we have to introduce the corresponding values of ω . Operating at the parallel resonant frequency the value of ω is

$$\omega = \omega_{op} \quad (13)$$

TABLE 4 Design data

Magnitude	Sym.	Equation	Operation frequency			Unit
			ω_{op}	ω_m	ω_o	
Frequency	f	(13)–(15)	450	460	481	kHz
Ind. ratio	β	(5)	3.4	5.2	6.9	
v_d to v_o phase	Φ	(11)	31.3	51.7	98.5	°
Ind. series	L_s	(5)	1.7	2.6	3.5	μH

If the inverter operates on the resonant frequency of the LLC resonant circuit, ω is [17]

$$\omega = \omega_o = \omega_{op} \sqrt{\frac{\beta + 1}{\beta}} \quad (14)$$

To obtain the intermediate frequency we must solve (4) for the frequency that fulfils the following equality [23].

$$\arg(Z(\omega_m)) = -\arcsin\left(\frac{1}{n}\right) \quad (15)$$

Assuming that the parallel equivalent R_p does not change appreciably in the range between ω_{op} and ω_o , it follows that the power of 25 kW is reached as long as the output voltage of the resonant circuit is kept at 460 V_{RMS} , which indicates that n remains constant. In this case, it is possible to solve (12) in each case to get the value of β that can be introduced in (11) to calculate ϕ , and in (5) to obtain L_s .

Table 4 shows the values of the design that results in each operation frequency.

By entering the values from Table 4 in (7), (9) and (10) the corresponding waveforms are obtained, which are shown in Figure 5.

Note that the value of the current in turn-on switching in all cases is negative (inductive commutation); therefore, zero voltage switching (ZVS) condition is achieved and most of the switching losses correspond to the turn-off switching.

4 | COMPARATIVE RESULTS

This section shows the results of a feature comparison over an inverter built with different transistor technologies and operating at different frequencies to choose the optimal design taking into account, mainly, the efficiency of the inverter. The comparative study is carried out using the results from the previous section shown in Table 5.

The inverter working at ω_o has a large output power factor because it requires a higher current to obtain the same output active power. This will decrease the inverter efficiency and increase the stress of its power components, so we could reject this operation mode. If the inverter operates in ω_{op} or ω_m the current values are similar and a more precise loss analysis is

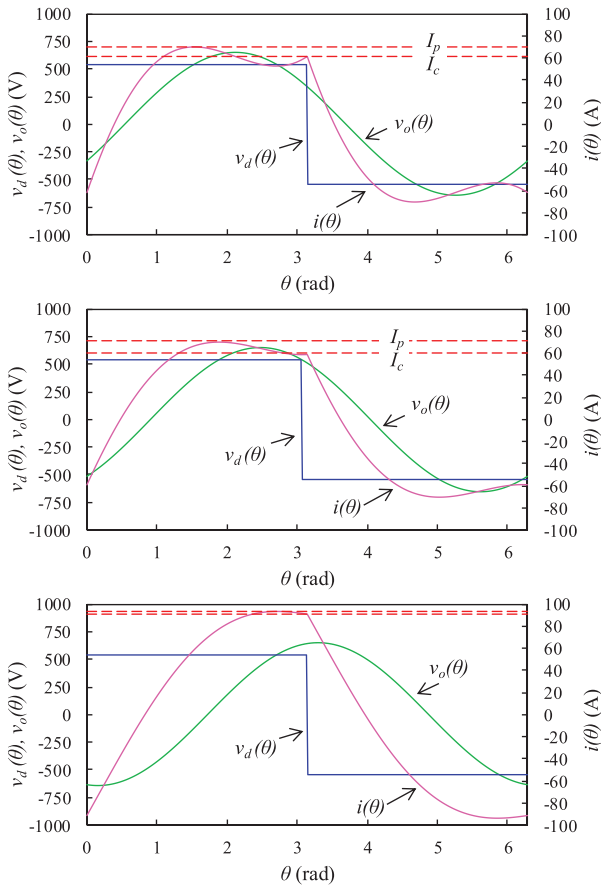


FIGURE 5 Waveforms of the LLC resonant inverter for ω_{op} (first row), ω_m (second row) and ω_o (third row). The blue curve corresponds to the inverter voltage $v_o(\theta)$, the magenta one to the output current $i(\theta)$ and the green one to the voltage of the parallel resonant circuit $v_d(\theta)$.

TABLE 5 Comparative results (i)

Magnitude	Sym.	Operation frequency			Unit
		ω_{op}	ω_m	ω_o	
Peak current	I_p	72	71	94	A
Switching current	I_c	61	60	91	A
v_d to i_o phase	$\arg(Z)$	21.8	29.2	50.9	°
RMS current	I_{RMS}	54.6	55.4	68.9	A

required to decide which of these two operating frequencies will be optimal.

4.1 | Output power, losses and efficiency analysis

In this sub-section, we have compared the power losses of the inverter for the chosen frequencies and for two types of transistors: Si insulated-gate bipolar transistor (IGBT) and SiC MOSFETs, which are currently very popular in power electronics applications.

The output power of the inverter is 25 kW and can be calculated, neglecting losses, using (16):

$$P_o = I_{RMS} \frac{nV_d}{\sqrt{2}} \cos(\arg Z(\omega)) \quad (16)$$

where ω must be taken the values derived from Equations (13) to (15).

A power losses analysis has been carried out considering the contribution of conduction losses (P_{cd}) and switching losses (P_{sw}) to total losses (P_{tot}) [6, 24]. For the analysis of P_{sw} , we will only take into account the turn-off losses of the inverter transistors because the turn-on switching losses are negligible due to ZVS condition.

The inverter is a full bridge that uses two units in parallel for each switch. The transistors chosen are the SiC MOSFET C3M0065100K of $V_{DS} = 1000$ V and $R_{DSon} = 65$ m Ω and the Si IGBT FGH75T65SHDTL4 of $V_{DS} = 650$ V and $V_{CE(sat)} = 1.6$ V that offers a good performance for high-frequency applications.

For MOSFETs, considering that both positive and negative current flow through the resistive channel, the conduction losses for each unit can be calculated using (17).

$$P_{cd} = \left(\frac{I_{RMS}}{2\sqrt{2}} \right)^2 R_{DSon} \quad (17)$$

For IGBTs, the conduction losses analysis must take into account that the positive current flows through the transistor while the negative current flows through the diode according to (18).

$$P_{cd} = \frac{1}{2\pi} \left(\int_0^{\arg(Z(\omega))} \frac{i(\theta)}{2} v_F d\theta + \int_{\arg(Z(\omega))}^{\pi} \frac{i(\theta)}{2} v_{CE(sat)} d\theta \right) \quad (18)$$

To make this calculation we can use a linear approximation of the transistor and diode direct characteristics. This means that the relations between the device drop voltage and current (v_F and i_F for the diode and v_{CE} and i_C for the transistor) are

$$v_F = k_1 i_\theta + k_2 \quad \text{and} \quad v_{CE(sat)} = k_3 i_\theta + k_4 \quad (19)$$

For the power device used in our inverter the values of the constants are: $k_1 = 0.016$ Ω , $k_2 = 0.9$ V, $k_3 = 0.006$ Ω and $k_4 = 1.2$ V.

On the other hand, it can calculate the switching power losses of both types of transistors using the curve of the turn-off switching energy E_{off} given by the manufacturer using the following polynomial function.

$$E_{off} = a I_c^2 + b I_c + c \quad (20)$$

TABLE 6 Losses and efficiency comparative results

Magnitude	Sym.	Operation frequency			Unit
		ω_{op}	ω_m	ω_o	
Conduction losses per transistor	P_{cd}	24.2	24.9	38.6	W
		20.2	20.2	23.9	
Switching losses per transistor	P_{sw}	23.6	22.7	52.0	W
		209.2	204.2	371.9	
Inverter total losses	P_{tot}	382.6	380.8	724.8	W
		1835.2	1795.2	3166.4	
Efficiency	η	98.5	98.5	97.1	%
		92.7	92.8	87.3	

where I_c is the transistor switching current and a , b and c take next values for each transistor type.

MOSFET	IGBT
$a = 0.0575 \mu\text{J} \text{A}^{-1/2}$	$a = 0.1352 \mu\text{J} \text{A}^{-1/2}$
$b = -0.585 \mu\text{J} \text{A}^{-1}$	$b = 10.62 \mu\text{J} \text{A}^{-1}$
$c = 16.25 \mu\text{J}$	$c = 11.74 \mu\text{J}$

Therefore, the switching turn-off losses can be calculated as

$$P_{sw} = E_{off} f \quad (21)$$

Since the inverter has eight transistors, to calculate the total power losses we use the next equation

$$P_{tot} = 8 (P_{cd} + P_{sw}) \quad (22)$$

The efficiency of the inverter can be calculated using (23).

$$\eta = \frac{P_o}{P_o + P_{tot}} \quad (23)$$

Table 6 shows the results of this loss analysis. The upper number of each cell corresponds to IGBT devices and the lower number to MOSFET devices. It is clearly appreciated that the conduced losses are similar but switching losses are reduced significantly due to the use of SiC MOSFET transistors, especially indicated for high-frequency applications [32].

Figure 6 shows graphically the results confirming that the use of SiC MOSFET transistors is preferred due to its low switching losses. Operating the inverter at ω_o causes higher power losses. This comparative study shows that working at ω_{op} or ω_m determines similar benefits in terms of power losses.

4.2 | Post-Curie behaviour analysis

During heating of a metallic material, the resistivity and, in the case of ferromagnetic loads, the permeability vary in a non-

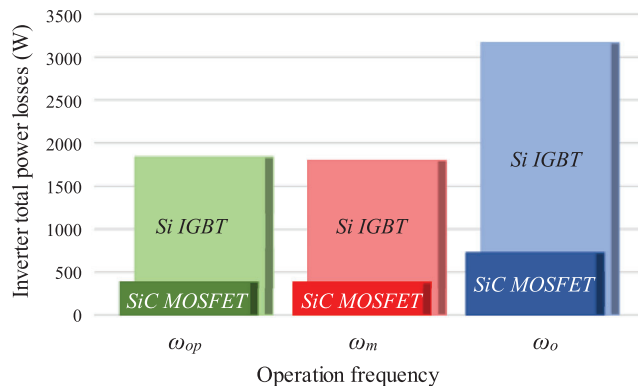


FIGURE 6 Comparison of the total inverter power losses with Si IGBT and SiC MOSFET working at three operation frequencies.

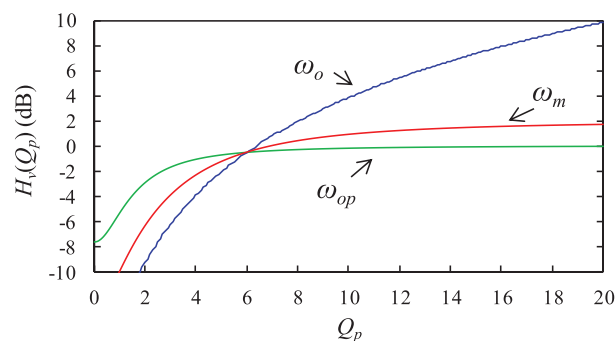


FIGURE 7 H_v in function of Q_p for different designs.

linear manner. This variation appears as a change in the values of R_p . For steel this change is dominated by the effects occurring at the Curie temperature (770°C), where the quality factor Q_p rapidly rises until values higher than 20 [22].

A large change in Q_p can cause over-voltages and over-currents at the inverter output that could only be prevented by a fast-responding control circuit varying the duty cycle of the switches to control the inverter output. For this reason, it would be preferable to choose the LLC inverter design, which is most insensitive to these changes. For this, a study of the evaluation of the voltage gain H_v must be carried out, solving (6) for various values of Q_p . Figure 7 shows the results of this study for each design where the gain is expressed in dB for a better understanding. It is observed that the operation of the LLC inverter working in ω_{op} is much more insensitive to changes in Q_p . This feature added to the result of the loss study implies that the ω_{op} must be the optimal operation frequency of the LLC inverter.

5 | INVERTER POWER CONTROL

There are various methods for regulating the voltage-fed inverters output power. In PFM [16], the output power can be controlled by varying the switching frequency while the inverter operates under a ZVS scheme. Other combined methods [25–27] and asymmetrical pulse width modulation [28] can be

used for LLC resonant converters. The PS control [29–31] is also applicable.

Using PFM in all LLC inverter designs the switching currents can be increased related to the RMS value of the current, decreasing unnecessarily the efficiency. In PS the phase ϕ between the conduction of the two legs of the full bridge allows varying the RMS value of the voltage applied to the resonant circuit and, hence, the output power. The reactive currents will circulate inversely through the transistors except for the necessary dead times. The next equations present $v_d(\theta)$ and $i(\theta)$ in the function of the PS ϕ .

$$v_d(\theta) = \begin{cases} 0 & \text{if } 0 \leq \theta < \phi \\ V_d & \text{if } \phi \leq \theta < \pi \\ 0 & \text{if } \pi \leq \theta < \pi + \phi \\ -V_d & \text{if } \pi + \phi \leq \theta < 2\pi \end{cases} \quad (24)$$

$$i(\theta) = \begin{cases} \frac{V_d}{L_s \omega} \left(n(\phi) \cos \left(\theta + \phi - \frac{\varphi}{2} \right) + \frac{\phi - \pi}{2} \right) & \text{if } 0 \leq \theta < \phi \\ \frac{V_d}{L_s \omega} \left(\theta + n(\phi) \cos \left(\theta + \phi - \frac{\varphi}{2} \right) - \frac{\pi + \varphi}{2} \right) & \text{if } \gamma - \pi + \varphi \leq \theta < \gamma \\ \frac{V_d}{L_s \omega} \left(n(\phi) \cos \left(\theta + \phi - \frac{\varphi}{2} \right) + \frac{\pi - \varphi}{2} \right) & \text{if } \gamma - \pi \leq \theta < \gamma + \varphi \\ \frac{-V_d}{L_s \omega} \left(\theta - n(\phi) \cos \left(\theta + \phi - \frac{\varphi}{2} \right) - \frac{3\pi + \varphi}{2} \right) & \text{if } \gamma + \varphi \leq \theta < \gamma + 2\pi \end{cases} \quad (25)$$

Both equations agree with Equations (9) and (10) for the case of $\phi = 0$. Note that the value of n is now not constant since V_p decreases as the RMS value of v_d decreases.

5.1 | Output power, losses and efficiency analysis with PS

The calculation of the output power is carried out with Equation (27) obtained analogously to Equation (16) taking into account the values of $n(\phi)$ that can be calculated as

$$n(\phi) = |H_v(\omega)| \frac{4}{\pi} \cos \left(\frac{\varphi}{2} \right) \quad (26)$$

and calculating $I_{RMS}(\phi)$ integrating (25).

$$P_o(\phi) = I_{RMS}(\phi) \frac{n(\phi) V_d}{\sqrt{2}} \cos(\arg Z(\omega)) \quad (27)$$

To calculate the inverter losses and the efficiency we use equations similar to (17) to (23) but taking into account that now the commutation current I_c depends on the PS. In addition, this current will take different values in the main branch (Q_1 and Q_3) and in the lagged branch (Q_2 and Q_4) [24]. Figure 8 shows the results of this loss analysis as a function of the output power.

It can be seen that the efficiency of the LLC inverter designs working in ω_{op} and ω_m is optimal since the I_{RMS} values and the switching currents are similar; however, the design working in

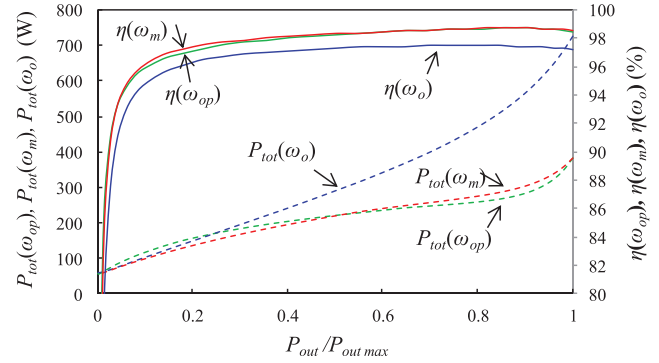


FIGURE 8 Evolution of the power losses and the efficiency of the inverter as a function of the output power.

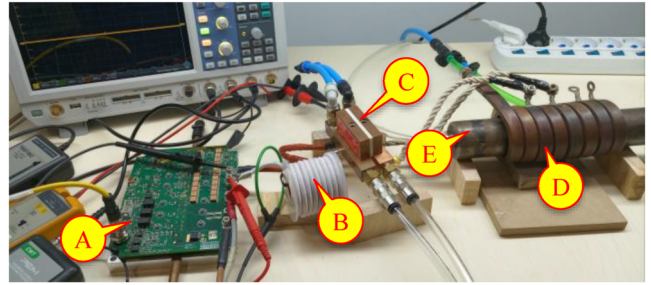


FIGURE 9 LLC inverter test bench. Labels indicate the items listed above.

ω_o has a lower efficiency since the conduction losses are higher and, mainly, the switching losses are much larger because of the switching current compared to the other designs. For this reason, this design could be discarded. It is important to highlight that working at high frequencies the operation of the inverter is possible thanks to the high performance of SiC MOSFET transistors compared to Si IGBT or Si MOSFET transistors [32].

5.2 | LLC inverter control strategies

Generally, inverters in induction heating applications work with constant power regulation. This is achieved by means of a feedback loop that compares the demanded power with the output power obtained as the mean value of the instantaneous multiplication of the output current and voltage. This loop acts on the PS control circuit [15].

To keep the inverter operating close to the designed frequency different algorithms must be used. For the design in ω_{op} , an oscillator circuit controlled by an integrator [24] can be used keeping the phase between the output capacitor voltage and the inverter output current near 0° . In the case of ω_o , a similar circuit must set the phase between the output voltage of the inverter and the inductor voltage [17] around 90° . Keeping the frequency close to ω_m is somewhat more complicated and requires the use of a minimum phase detector circuit [23].

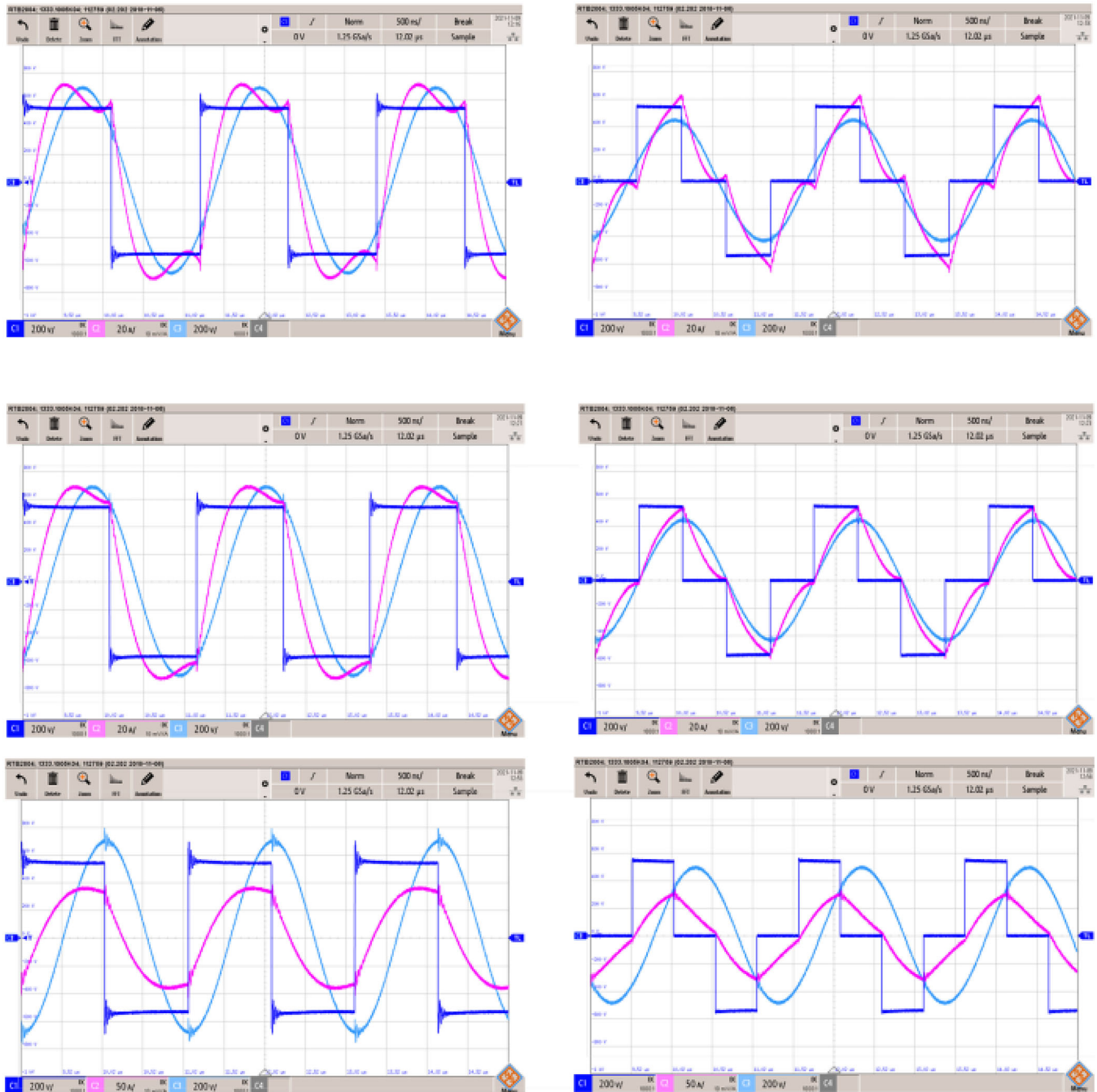


FIGURE 10 Experimental waveforms of the LLC inverter for ω_p (first row), ω_m (second row) and ω_s (third row) working at full power (left column) and with phase-shift of 90° (right column). C1 (dark blue) is the output voltage (200 V/div), C2 (magenta) is the output current (20 A/div for ω_p and ω_m and 50 A/div for ω_s) and C3 (light blue) is the inductor voltage (200 V/div). Time base is 500 ns/div.

6 | EXPERIMENTAL RESULTS

This section shows the experimental results that have been obtained testing a 25-kW power prototype working at a frequency higher than 450 kHz. The inverter was powered by a 540 V DC voltage source. The values of the components of the resonant circuit are those obtained in Sections 2 and 3. In order

to verify experimentally the design, a test setup has been made with these elements:

- A. A complete inverter bridge with eight SiC C3M0065100K MOSFETs with an integrated digital electronic control on an FPGA-based system mounted on a water cooling heatsink.

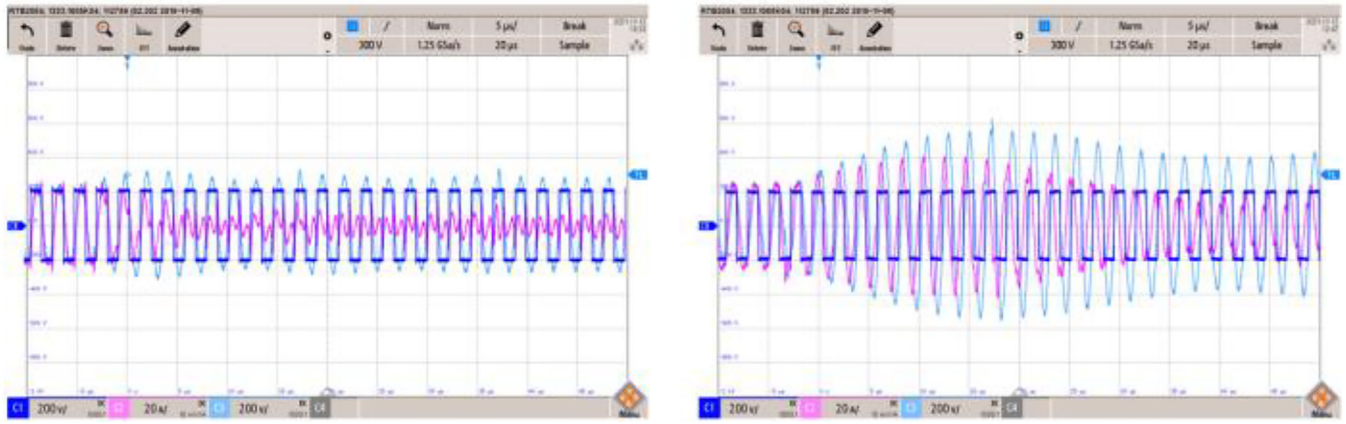


FIGURE 11 Experimental waveforms of the LLC inverter with change of Q_p from 6 to 20. Left waveforms correspond to the design in ω_{op} . Right waveforms correspond to the design in ω_m . C1 (dark blue) is the output voltage (200 V/div), C2 (magenta) is the output current (20 A/div) and C3 (light blue) is the inductor voltage (200 V/div). Time base is 5 μ s/div.

- B. A set of 1.7, 2.6 and 3.5 μ H inductors compound with Litz wire.
- C. A high-power capacitor of 0.25 μ F usable for induction heating.
- D. A water-cooled solenoidal heating inductor of 0.5 μ H.
- E. A water-cooled test dummy load.

Figure 9 shows a picture of the test bench used to obtain the following experimental results. Note that the design of the heating inductor and the work-piece have been amended from those described in Section 2 to allow long-term tests.

Figure 10 shows digital storage oscilloscope (DSO) measurements of the main waveforms of the LLC inverter for different designs operating at full power (left) and with a PS of 90° (right). The expected output voltage, current, power and frequency values have been obtained with sufficient accuracy despite the dispersion of the real values of the components used.

To test experimentally how the inverter output behaves with changes in Q_p , the following waveforms have been captured when part of the load is quickly extracted from inside the inductor in order to implement a change of Q_p from 6 to approximately 20. The input DC voltage was reduced to 200 V to prevent overvoltages. It is verified that the changes of the resonant circuit output voltage correspond to those foreseen in Section 4. This experiment has not been carried out with design in ω_o , which would have to withstand too large voltage changes. Figure 11 shows the obtained experimental results.

The amplitude of the inverter output current decreases for the design in ω_{op} while it increases in the other case that would only lead to a temporary overheating of the power components. On the other hand, the amplitude of the output voltage increases slightly for the ω_{op} design while it increases with a factor close to 2 for the case of design in ω_m . This situation would persist for some time until the power feedback control corrects the inverter duty cycle; meanwhile, the capacitors of

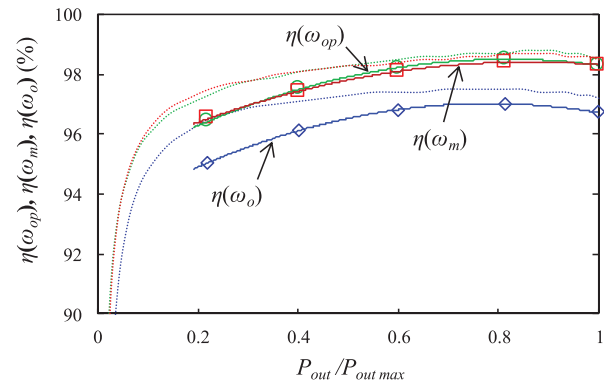


FIGURE 12 Experimental output power and efficiency of LLC inverter in function of output power. The dashed lines represent the calculations and the marking symbols represent the experimental measurements.

the LLC circuit could be damaged due to overvoltage. These results confirm that the ω_{op} design is preferable.

Figure 12 shows the experimental and calculated measures of efficiency. Note that the efficiency is greater than 98% for designs in ω_{op} and ω_m . The differences that are observed are due to the existence of other losses that have not been considered and to the error of the measurement process.

7 | CONCLUSIONS

This article proposed how an LLC inverter can be used more efficiently if the operating frequency is close to the resonance of the parallel resonant circuit. A complete design procedure has been presented that allows designing an LLC resonant inverter for a given application. A novel method has been shown to find the working conditions corresponding to the LLC designs in three singular operating frequencies. A comparative study has been carried out to choose the optimal design consisting of

an LLC inverter that works at the parallel resonant frequency. Under these conditions, there will be less current stress on the resonant circuit components and through connections. At the same time, the conduction and switching losses are minimized and the efficiency of the converter is maximized. In addition, this design provides a good behaviour against large load changes with a reduced dimensioning of the series inductor.

An inverter output power control technique based on PS modulation has also been presented. Its application has made it possible to evaluate the evolution of the efficiency of the inverter against the output power of the inverter. The viability of this design has been verified with the construction and test of a 25-kW LLC inverter using SiC MOSFET transistors in a high-frequency induction heating application.

AUTHOR CONTRIBUTIONS

Vicente Esteve: Conceptualization; validation; writing original draft; writing review and editing. Jose Jordán: Conceptualization; validation. Enrique J. Dede: Conceptualization, resources. Pedro J. Martinez and Kevil J. Ferrara: Validation. Juan L. Bellido: Software, validation.

CONFLICT OF INTEREST STATEMENT

The authors declare no conflict of interest.

DATA AVAILABILITY STATEMENT

Data sharing not applicable—no new data generated, or the article describes entirely theoretical research.

ORCID

Vicente Esteve  <https://orcid.org/0000-0002-0692-5413>

REFERENCES

- Lucía, O., Maussion, P., Dede, E.J., Burdío, J.M.: Induction heating technology and its applications: Past developments, current technology, and future challenges. *IEEE Trans. Ind. Electron.* 61(5), 2509–2520 (2014)
- Rudnev, V., Loveless, D., Cook, R., Black, M.: *Hand Book of Induction Heating*. CRC Press, Boca Raton, Florida (2017)
- Brown, G.H., Hoyle, C.N., Bierwirth, R.A.: *Theory and Application of Radio-Frequency Heating*. Van Nostrand, New York (1947)
- Park, N.-J., Lee, D.-Y., Hyun, D.-S.: A power-control scheme with constant switching frequency in class-d inverter for induction-heating jar application. *IEEE Trans. Ind. Electron.* 54(3), 1252–1260 (2007)
- Faucher, S., Forest, F., Gaspard, J.-Y., Huselstein, J.-J., Joubert, C., Montloup, D.: Frequency-synchronized resonant converters for the supply of multiwinding coils in induction cooking appliances. *IEEE Trans. Ind. Electron.* 54(1), 441–452 (2007)
- Lucía, O., Burdío, J.M., Millán, I., Acero, J., Barragán, L.A.: Efficiency oriented design of ZVS half-bridge series resonant inverter with variable frequency duty cycle control. *IEEE Trans. Power Electron.* 25(7), 1671–1674 (2010)
- Yilmaz, İ., Ermis, M., Cadirci, I.: Medium-frequency induction melting furnace as a load on the power system. *IEEE Trans. Ind. Appl.* 48(4), 1203–1214 (2012)
- Shenkman, A., Axelrod, B., Chudnovsky, V.: Assuring continuous input current using a smoothing reactor in a thyristor frequency converter for induction metal melting and heating applications. *IEEE Trans. Ind. Electron.* 48(6), 1290–1292 (2001)
- Kawashima, R., Mishima, T., Ide, C.: Three-phase to single-phase multiresonant direct AC–AC converter for metal hardening high-frequency induction heating applications. *IEEE Trans. Power Electron.* 36(1), 639–653 (2021)
- Barragán, L.A., Navarro, D., Acero, J., Urriza, I., Burdío, J.M.: FPGA implementation of a switching frequency modulation circuit for EMI reduction in resonant inverters for induction heating appliances. *IEEE Trans. Ind. Electron.* 55(1), 11–20 (2008)
- Lucía, O., Burdío, J.M., Millán, I., Acero, J., Puyal, D.: Load-adaptive control algorithm of half-bridge series resonant inverter for domestic induction heating. *IEEE Trans. Ind. Electron.* 56(8), 3106–3116 (2009)
- Namadmalan, A.: Universal tuning system for series-resonant induction heating applications. *IEEE Trans. Ind. Electron.* 64(4), 2801–2808 (2017)
- Meziane, B., Zeroug, H.: Comprehensive power control performance investigations of resonant inverter for induction metal surface hardening. *IEEE Trans. Ind. Electron.* 63(10), 6086–6096 (2016)
- Guillén, P., Sarnago, H., Lucía, O., Burdío, J.M.: Mains-synchronized pulse density modulation strategy applied to a ZVS resonant matrix inverter. *IEEE Trans. Ind. Electron.* 68(11), 10835–10844 (2021)
- Esteve, V., Sanchis-Kilders, E., Jordan, J., Dede, E.J., Cases, C., Maset, E., Ejea, J.B., Ferreres, A.: Improving the efficiency of IGBT series-resonant inverters using pulse density modulation. *IEEE Trans. Ind. Electron.* 58(3), 979–987 (2011)
- Yamamoto, J., Zaitso, T., Abe, S., Ninomiya, T.: PFM and PWM hybrid controlled LLC converter. In: *Proceedings of IEEE International Power Electronics Conference*, pp. 177–182 (2014)
- Espí, J.M., Dede, E.J., García-Gil, R., Castelló, J.: Design of the L-LC resonant inverter for induction heating based on its equivalent SRI. *IEEE Trans. Ind. Electron.* 54(6), 3178–3187 (2007)
- Ngo-Phi, T., Nguyen-Quang, N.: LLC inverter design procedure for induction heating with quantitative analysis of power transfer. *Sci. Tech. Dev. J. Eng. Technol.* 4, 738–746 (2021)
- Davies, J., Simpson, P.: *Induction Heating Handbook*. McGraw-Hill, New York (1979)
- Wheeler, H.A.: Discussion on simple inductance formulas for radio coils. *Proc. Inst. Radio Eng.* 17(3), 580–582 (1929)
- Wheeler, H.A.: Inductance formulas for circular and square coils. *Proc. IEEE* 70(12), 1449–1450 (1982)
- Sewell, H.L., Stone, D.A., Bingham, C.M.: Dynamic load impedance matching for induction heater systems. *COMPEL* 22(1), 30 (2003)
- Esteve, V., et al.: Optimal LLC inverter design with SiC MOSFETs and phase shift control for induction heating applications. *IEEE Trans. Ind. Electron.* 69(11), 11100–11111 (2022)
- Esteve, V., Jordan, J., Sanchis Kilders, E., Dede, E., Maset, E., Ejea, J., et al.: Improving the reliability of series resonant inverters for induction heating applications. *IEEE Trans. Ind. Electron.* 61, 2564–2572 (2014)
- Park, H.-P., Jung, J.-H.: PWM and PFM hybrid control method for LLC resonant converters in high switching frequency operation. *IEEE Trans. Ind. Electron.* 64(1), 253–263 (2017)
- Ahmed, N.: High frequency soft switching AC conversion circuit with dual mode PWM/PDM control strategy for high power IH applications. *IEEE Trans. Ind. Electron.* 58(4), 1440–1448 (2011)
- Dudrik, J., Trip, N.-D.: Soft-switching PS-PWM DC–DC converter for full-load range applications. *IEEE Trans. Ind. Electron.* 57(8), 2807–2814 (2010)
- Chudjuarjeen, S., Sangswang, A., Koopai, C.: An improved LLC resonant inverter for induction-heating applications with asymmetrical control. *IEEE Trans. Ind. Electron.* 58(7), 2915–2925 (2011)
- Ye, Z., Jain, P.K., Sen, P.C.: A two-stage resonant inverter with control of the phase angle and magnitude of the output voltage. *IEEE Trans. Ind. Electron.* 54(5), 2797–2812 (2007)
- Lo, Y.K., Lin, C.Y., Hsieh, M.T., Lin, C.Y.: Phase-shifted full-bridge series-resonant DC–DC converters for wide load variations. *IEEE Trans. Ind. Electron.* 58(6), 2572–2575 (2011)

31. Showybul, S.M., Shakib, I., Mekhilef, S.: A frequency adaptive phase shift modulation control-based LLC series resonant converter for wide input voltage applications. *IEEE Trans. Power Electron.* 32(11), 8360–8370 (2017)
32. Mikamura, Y., Hiratsuka, K., Tsuno, T., Michikoshi, H., Tanaka, S., Masuda, T., Wada, K., Horii, T., Genba, J., Hiyoshi, T., Sekiguchi, T.: Novel designed SiC devices for high power and high efficiency systems. *IEEE Trans. Electron Devices* 62(2), 382–389 (2015)

How to cite this article: Esteve, V., Jordán, J., Dede, E.J., Martínez, P.J., Ferrara, K.J., Bellido, J.L.: Comparative analysis and improved design of LLC inverters for induction heating. *IET Power Electron.* 16, 1754–1764 (2023). <https://doi.org/10.1049/pel2.12484>